Electronic Supporting Information (ESI):

Blend for All or Pure for Few?
Well-to-Wheel Life Cycle Assessment of Blending Electricity-Based OME_{3-5} With Fossil Diesel

Simon Voelker[a], *Sarah Deutz*[a], *Jannik Burre*[b], *Dominik Bongartz*[b], *Ahmad Omari*[c], *Bastian Lehrheuer*[c], *Alexander Mitsos*[d,b,f], *Stefan Pischinger*[c], *André Bardow*[a,d,e,f], *and Niklas von der Assen*[a,*]

[a] *Institute of Technical Thermodynamics, RWTH Aachen University, Aachen 52062, Germany*
[b] *Process Systems Engineering, RWTH Aachen University, Aachen 52074, Germany*
[c] *Institute for Combustion Engines, RWTH Aachen University, Aachen 52074, Germany*
[d] *JARA-ENERGY, 52056 Aachen, GERMANY*
[e] *Energy & Process Systems Engineering, ETH Zurich, Zürich 8092, Switzerland*
[f] *Energy Systems Engineering (IEK-10), Forschungszentrum Jülich, Jülich 52425, Germany*
[*] *Corresponding author: niklas.vonderassen@ltt.rwth-aachen.de*

S1 Well-to-tank: OME_{3-5} production processes (worst-case scenario)

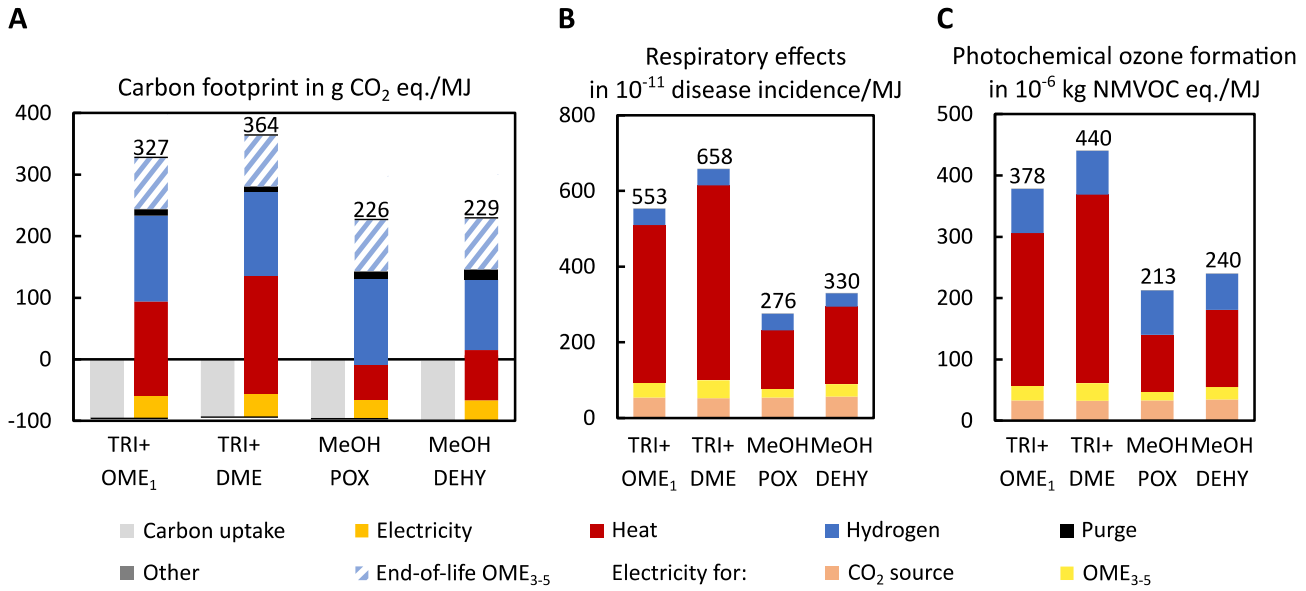

Figure S1: Well-to-tank (A) carbon footprint in g CO_2 eq. per MJ, (B) respiratory effects in 10^{-11} disease incidence per MJ, and (C) photochemical ozone formation in 10^{-6} kg NMVOC eq. per MJ of the four OME_{3-5} production routes for the worst-case scenario. The carbon footprint of the carbon uptake due to CO_2 utilization is negative (light grey). Positive environmental impacts result from direct CO_2 emissions in purge gases from OME_{3-5} production (black), electricity supply (yellow) that is further subdivided in electricity for OME_{3-5} and CO_2 supply in (B) and (C), other emissions due to process water supply and wastewater treatment (dark grey), heat supply (red), and hydrogen supply (blue). Although not inside the system boundary of a well-to-tank analysis, we additionally indicate the end-of-life emissions from OME_{3-5} combustion for the carbon footprint (A, hatched blue): The entire life cycle of CO_2-based fuels cannot be carbon-negative and is thus carbon-neutral at best.

S2 Well-to-tank: OME_{3-5} production processes (best-case scenario with CO_2 from direct air capture)

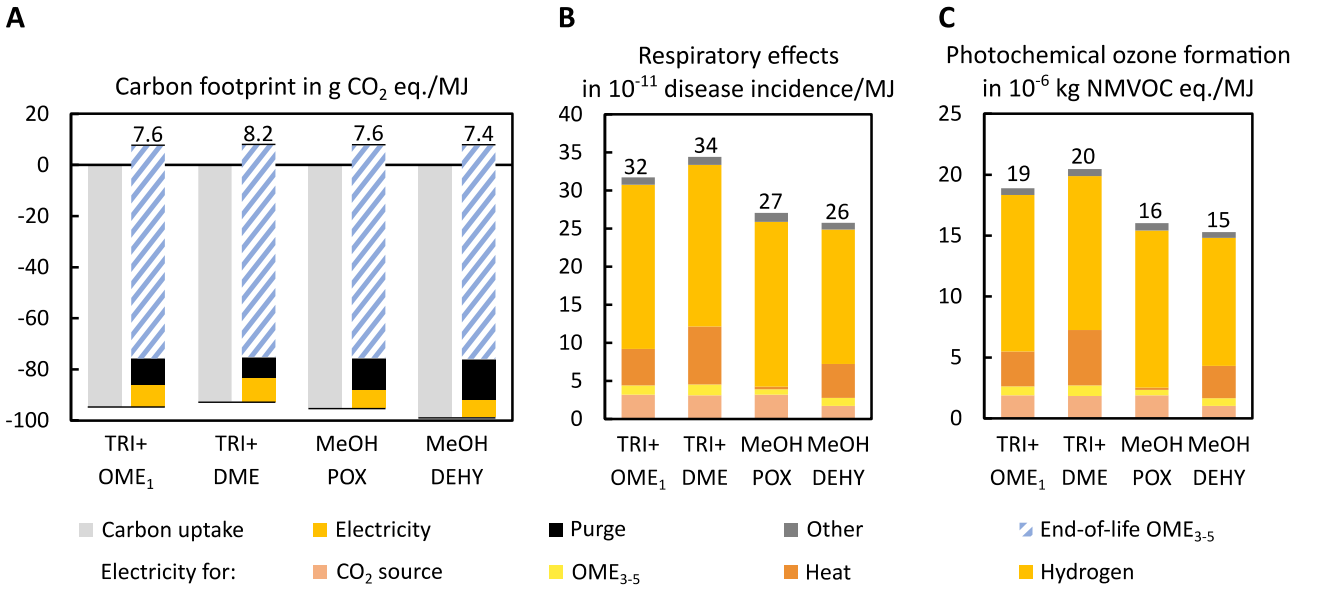

Figure S2: Well-to-tank (A) carbon footprint in g CO_2 eq. per MJ, (B) respiratory effects in 10^{-11} disease incidence per MJ, and (C) photochemical ozone formation in 10^{-6} kg NMVOC eq. per MJ of the four OME_{3-5} production routes for the best-case scenario but now with CO_2 from direct air capture. The carbon footprint of the carbon uptake due to CO_2 utilization is negative (light grey). Positive environmental impacts result from direct CO_2 emissions in purge gases from OME_{3-5} production (black), minor emissions due to process water supply and wastewater treatment (dark grey), and electricity supply (yellow). The electricity supply is further subdivided in electricity for hydrogen, heat, OME_{3-5}, and CO_2 supply in (B) and (C). Although not inside the system boundary of a well-to-tank analysis, we additionally indicate the end-of-life emissions from OME_{3-5} combustion for the carbon footprint (A, hatched blue): The entire life cycle of CO_2-based fuels cannot be carbon-negative and is thus carbon-neutral at best.

S3 Well-to-wheel: the entire life cycle of diesel-OME_{3-5} blends (worst-case scenario)

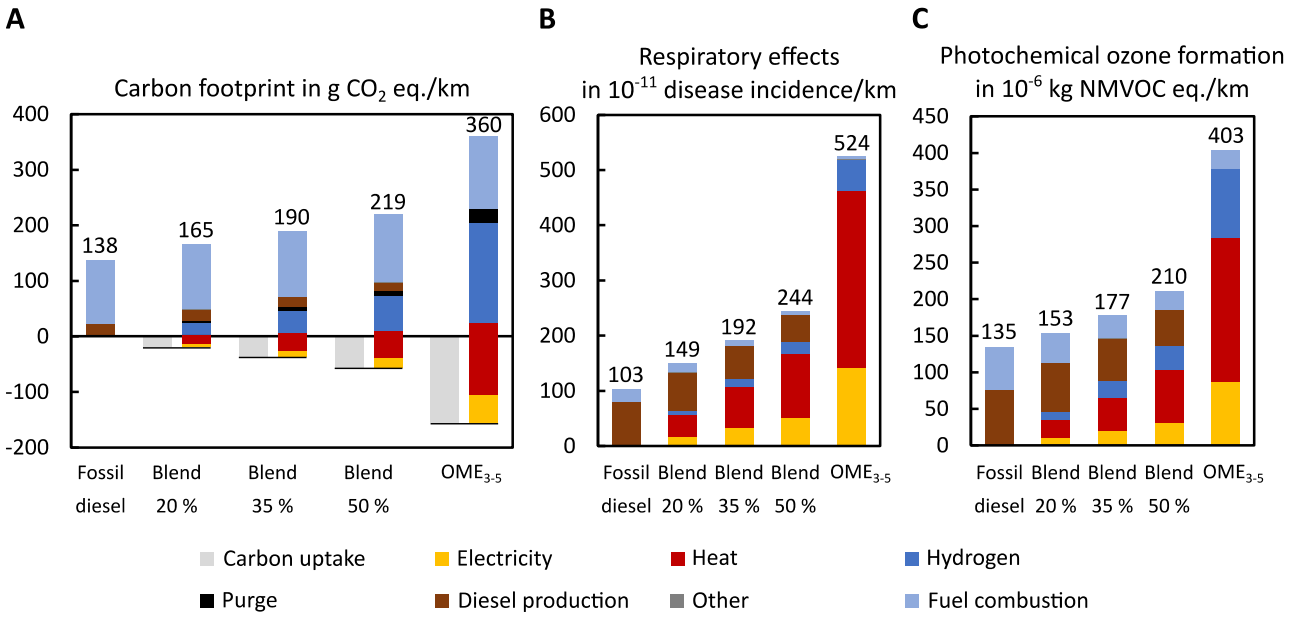

Figure S3: Well-to-wheel (A) carbon footprint in g CO_2 eq. per km, (B) respiratory effects in 10^{-11} disease incidence per km, and (C) photochemical ozone formation in 10^{-6} kg NMVOC eq. per km of pure fossil diesel, blends of OME_{3-5} in fossil diesel, and pure OME_{3-5} for the worst-case scenario. OME_{3-5} is produced via the MeOH DEHY route. The carbon footprint of the carbon uptake due to CO_2 utilization is negative (light grey). Positive environmental impacts result from electricity supply (yellow), heat supply (red), hydrogen supply (dark blue), direct CO_2 emissions in purge gases from OME_{3-5} production (black), diesel production (brown), fuel combustion (light blue), and other environmental impacts due to process water supply and wastewater treatment (dark grey).

S4 Well-to-wheel: the entire life cycle of diesel-OME_{3-5} blends (best-case scenario with CO_2 from direct air capture)

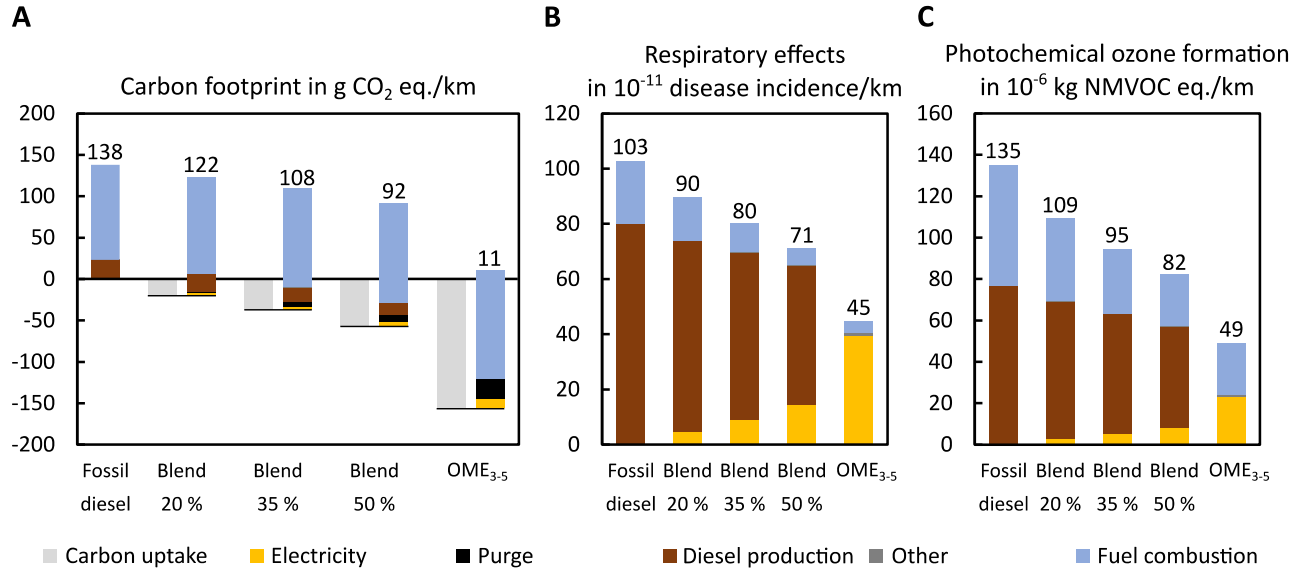

Figure S4: Well-to-wheel (A) carbon footprint in g CO_2 eq. per km, (B) respiratory effects in 10^{-11} disease incidence per km, and (C) photochemical ozone formation in 10^{-6} kg NMVOC eq. per km of pure fossil diesel, blends of OME_{3-5} in fossil diesel, and pure OME_{3-5} for the best-case scenario but now with CO_2 from direct air capture. OME_{3-5} is produced via the MeOH DEHY route. The carbon footprint of the carbon uptake due to CO_2 utilization is negative (light grey). Positive environmental impacts result from electricity supply (yellow), direct CO_2 emissions in purge gases from OME_{3-5} production (black), diesel production (brown), fuel combustion (light blue), and minor emissions due to process water supply and wastewater treatment (dark grey).

S5 Blending OME_{3-5} gradually into a fleet

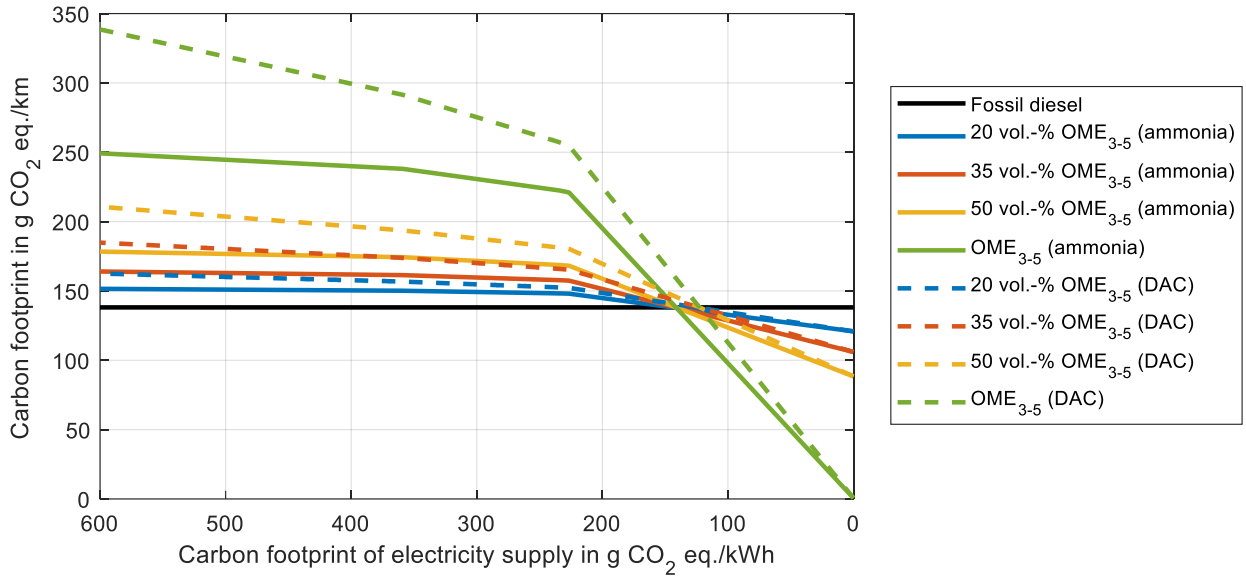

Figure S5: The well-to-wheel carbon footprint as function of the carbon footprint of electricity supply for pure OME_{3-5}, blends of 20, 35, and 50 vol.-% OME_{3-5} in diesel as well as pure fossil diesel. Results are shown for CO_2 from an ammonia plant (solid curves) and for CO_2 from direct air capture (dashed curves). The well-to-wheel impacts include emissions along the entire life cycle of diesel-OME_{3-5} blends.

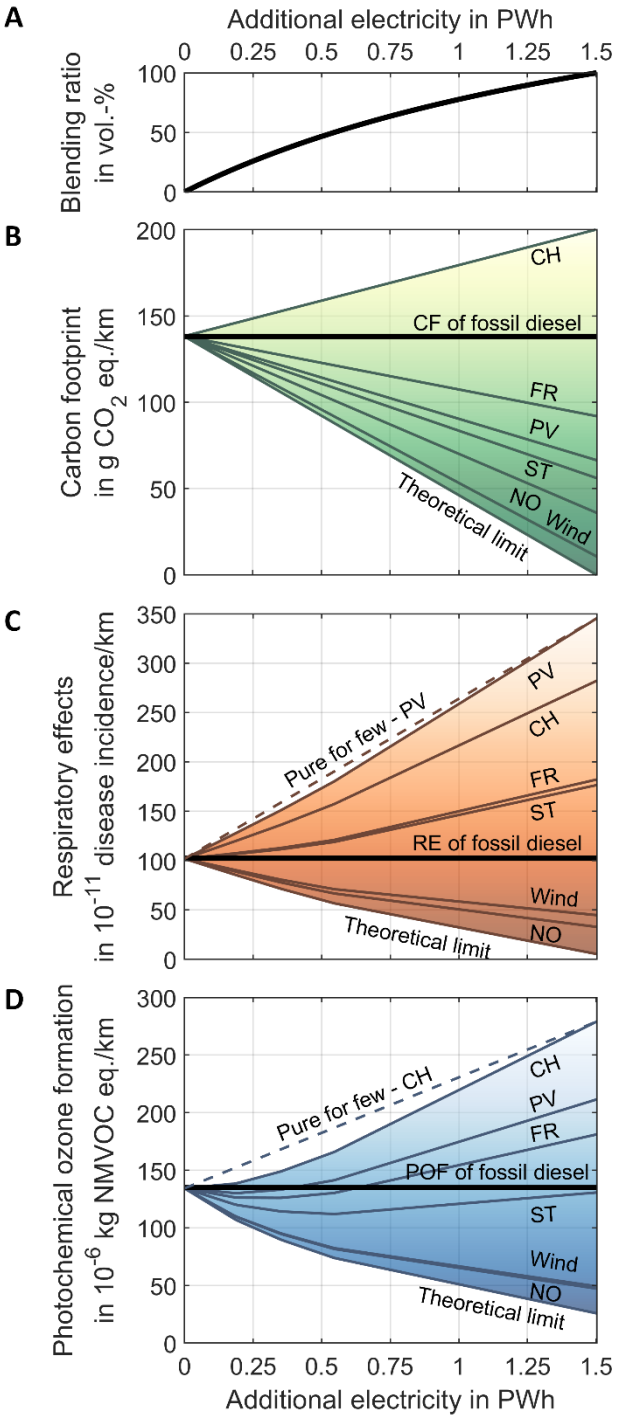

Figure S6: (A) The volumetric blending ratio, the well-to-wheel (B) carbon footprint (CF), (C) respiratory effects (RE), and (D) photochemical ozone formation (POF) as function of additionally available electricity for OME_{3-5} production. Results are presented for country- and technology-specific environmental impacts of electricity. Solid curves indicate the environmental impacts of blending OME_{3-5} with fossil diesel for the entire fleet ("blend for all"), while dashed lines show the results for switching only some diesel passenger cars to pure OME_{3-5} usage ("pure for few"). "Pure for few" is the linear combination of pure diesel and pure OME_{3-5} and is, for the sake of better readability, shown for only two examples. The black bold lines indicate the environmental impacts of pure fossil diesel for reference. CO_2 is supplied by direct air capture. CH: Switzerland, FR: France, NO: Norway, PV: photovoltaic, and ST: solar-thermal. The theoretical limit of a burden-free electricity supply is also included as lower bound.

S6 Life cycle inventories

In this section, life cycle inventories (LCI) of all OME_{3-5} production routes and the life cycle assessment (LCA) datasets for the background system are presented. LCIs for OME_{3-5} production routes are shown as modified for our analyses and as heat-integrated. Heat integrations have been performed or recalculated, where necessary due to our modifications (cf. Section 3 in the manuscript).

Characteristics of anhydrous and aqueous OME_{3-5} routes

Dependent on whether water coexists in the final process step of OME_{3-5} formation, OME_{3-5} routes can be divided into two types: anhydrous and aqueous routes (cf. Figure 2 in the manuscript). In the aqueous routes, the production of water during OME_{3-5} production is disadvantageous. First, it lowers the OME_{3-5} yield as undesired side products are formed [1] and equilibrium conversion is shifted towards the reactants. [2] Second, water complicates product separation due to similar physio-chemical properties between water and OME_2 and the formation of azeotropes. [3] Promising solutions for water removal, e.g., membranes, are however in investigation. [4] An advantage of the aqueous routes is the direct use of methanol and formaldehyde (FA) for the production of OME_{3-5}. The anhydrous routes are advantageous as water is absent during OME_{3-5} formation, making both the reaction and the separation of the final product less complicated. However, a water-free FA source, e.g., trioxane or anhydrous FA, is required, whose production is energy-intensive. [5]

Consistency in the underlying modelling assumptions for the considered OME_{3-5} routes

Using data from different authors in a comparative study requires thorough consideration of consistency in the underlying modelling assumptions. Given the following model characteristics, we can conclude that the assumptions of the different process models are similar enough for a comparison. For the reactor models, we used detailed kinetic models where available (methanol, formaldehyde via partial oxidation of methanol, OME_1, OME_{3-5} from trioxane and OME_1, and OME_{3-5} from methanol and formaldehyde). Where no detailed kinetic models were available, we used either industrial data (trioxane), experimental data (formaldehyde via dehydrogenation of methanol), or equilibrium-based models if the process is experimentally or industrially close to equilibrium (DME, and OME_{3-5} from trioxane and DME). For distillation columns, tray-to-tray RadFrac models were used everywhere. Overall, the thermodynamic models are based on the work of one research group (Maurer, Albert, Hasse, and Burger), which again speaks for a certain consistency between the models. Finally, for all routes, we recalculated or calculated for the first time, where not yet done in literature, pinch-based heat integration to further improve comparability between the routes.

Anhydrous OME_{3-5} route via trioxane and OME_1 (TRI+OME_1)

Trioxane is the most common intermediate for anhydrous OME_{3-5} production. It is commonly produced industrially from aqueous FA with a low FA conversion of approximately 5 % catalyzed by sulfuric acid. [6] To achieve a high overall trioxane yield, high recycle streams are necessary, which result in a high energy demand for separation both

by pure distillation [6] and by the conventional but more complex extractive distillation. [7] The capping source for anhydrous OME_{3-5} production can either be OME_1 or dimethyl ether (DME) (cf. Figure 2 in the manuscript).

OME_{3-5} production via trioxane and OME_1 (TRI+OME_1) is the most well-known anhydrous route. OME_1 can be produced from methanol and aqueous FA using established process concepts with an acidic catalyst and a reactive pressure-swing distillation. [8] In OME_{3-5} formation, trioxane first decomposes over an acidic catalyst to molecular FA, which is then incorporated into OME_{n-1}. [9] An alternative mechanism is the direct incorporation of trioxane into OME_{n-3}. A high selectivity towards OME_{3-5} of approximately 70 % can be achieved and its purification via rectification requires only little energy. [10–14]

Table S1: Life cycle inventory of methanol production[15] for the anhydrous route via trioxane and OME_1 (TRI+OME_1) with full heat integration per kg of OME_{3-5}.

Flow		Value	Unit
In			
	H_2	-0.249	kg
	CO_2	-1.816	kg
	Air	-0.676	kg
	Electricity	-1.270	MJ
Out			
	Methanol	1.272	kg
	Exhaust	0.746	kg
	thereof CO_2	0.065	kg

Table S2: Life cycle inventory of formaldehyde production[15] for the anhydrous route via trioxane and OME_1 (TRI+OME_1) with full heat integration per kg of OME_{3-5}.

Flow		Value	Unit
In			
	Methanol	-0.850	kg
	Water	-0.318	kg
	Water, solvent	-0.080	kg
	Air	-2.275	kg
	Electricity	-0.155	MJ
Out			
	Formaldehyde, aq (50 wt.-%)	1.446	kg
	Exhaust	2.078	kg
	thereof CO_2	0.103	kg

Table S3: Life cycle inventory of OME_1 production[15] for the anhydrous route via trioxane and OME_1 (TRI+OME_1) with full heat integration per kg of OME_{3-5}.

Flow		Value	Unit
In			
	Methanol	-0.422	kg
	Formaldehyde, aq (50 wt.-%)	-0.394	kg
	Air	-0.338	kg
	Electricity	-0.001	MJ
Out			
	OME_1	0.484	kg
	Wastewater	0.316	kg
	Exhaust	0.355	kg
	thereof CO_2	0.028	kg

Table S4: Life cycle inventory of trioxane production[16] for the anhydrous route via trioxane and OME_1 (TRI+OME_1) with full heat integration per kg of OME_{3-5}.

Flow		Value	Unit
In			
	Formaldehyde, aq (50 wt.-%)	-1.052	kg
	Electricity	-1.036	MJ
	Heat at 93°C	-13.265	MJ
	Heat at 128°C	-5.165	MJ
Out			
	Trioxane	0.515	kg
	Wastewater	0.536	kg

Table S5: Life cycle inventory of OME_{3-5} production[16] for the anhydrous route via trioxane and OME_1 (TRI+OME_1) with full heat integration per kg of OME_{3-5}.

Flow		Value	Unit
In			
	OME_1	-0.484	kg
	Trioxane	-0.515	kg
Out			
	OME_{3-5}	1.000	kg

Anhydrous OME_{3-5} route via trioxane and DME (TRI+DME)

The advantage of producing OME_{3-5} via trioxane and DME (TRI+DME) is the more direct access to DME from H_2 and CO_2 compared to OME_1. Thereby, the methanol and FA production plants are only needed for trioxane production and can thus be smaller. DME can be produced directly from H_2 and CO_2 [17] in a one-step process without producing methanol as an intermediate. [18] For OME_{3-5} production from trioxane and DME, a higher energy demand is reported compared to OME_{3-5} production from trioxane and OME_1, while the production of DME is highlighted as cheaper compared to OME_1. [19]

Table S6: Life cycle inventory of methanol production[15] for the anhydrous route via trioxane and DME (TRI+DME) with full heat integration per kg of OME_{3-5}.

Flow	Value	Unit
In		
H_2	-0.169	kg
CO_2	-1.227	kg
Air	-0.457	kg
Electricity	-0.858	MJ
Out		
Methanol	0.860	kg
Exhaust	0.504	kg
thereof CO_2	0.044	kg

Table S7: Life cycle inventory of formaldehyde production[15] for the anhydrous route via trioxane and DME (TRI+DME) with full heat integration per kg of OME_{3-5}.

Flow	Value	Unit
In		
Methanol	-0.860	kg
Water	-0.322	kg
Water, solvent	-0.081	kg
Air	-2.301	kg
Electricity	-0.157	MJ
Out		
Formaldehyde, aq (50 wt.-%)	1.463	kg
Exhaust	2.102	kg
thereof CO_2	0.104	kg

Table S8: Life cycle inventory of DME production[20] for the anhydrous route via trioxane and DME (TRI+DME) with full heat integration per kg of OME_{3-5}.

Flow	Value	Unit
In		
H_2	-0.076	kg
CO_2	-0.552	kg
Air	-0.091	kg
Electricity	-0.409	MJ
Out		
DME	0.284	kg
Wastewater	0.334	kg
Exhaust	0.101	kg
thereof CO_2	0.009	kg

Table S9: Life cycle inventory of trioxane production[16] for the anhydrous route via trioxane and DME (TRI+DME) with full heat integration per kg of OME_{3-5}.

Flow		Value	Unit
In			
	Formaldehyde, aq (50 wt.-%)	-1.463	kg
	Electricity	-1.440	MJ
	Heat at 93°C	-15.627	MJ
	Heat at 128°C	-9.772	MJ
Out			
	Trioxane	0.716	kg
	Wastewater	0.745	kg

Table S10: Life cycle inventory of OME_{3-5} production[19] for the anhydrous route via trioxane and DME (TRI+DME) with full heat integration per kg of OME_{3-5}.

Flow		Value	Unit
In			
	DME	-0.284	kg
	Trioxane	-0.716	kg
Out			
	OME_{3-5}	1.000	kg

Aqueous OME_{3-5} route via methanol and formaldehyde by partial oxidation of methanol (MeOH POX)

In contrast to the anhydrous routes, aqueous routes directly utilize methanol and typically aqueous FA for OME_{3-5} formation (cf. Figure 2 in the manuscript). In addition to the complex oligomerization reactions in methanolic and aqueous FA solutions, which take place without the presence of a catalyst, [21] the desired formation of OME_n takes place in the presence of an acidic catalyst accompanied by water formation following etherification reactions. [22] The alternative chain-growth mechanism of OME_1 towards OME_n is the direct incorporation of FA into OME_{n-1}. Irrespective of the mechanism, water is present in the system. However, the amount of water and thus the type of FA source may have a huge influence on the performance of the OME_{3-5} production.

Commercial FA production takes place via partial oxidation of methanol (FORMOX process) or combined partial oxidation and dehydrogenation of methanol (BASF process). [5] In the BASF process, co-produced H_2 is burned for power generation since it is diluted in the remaining off-gas. For both processes, the overall reaction stoichiometry is the same and the resulting FA concentration in the aqueous solution is up to 55 wt.-%. [5] To increase the FA concentration, a subsequent falling-film evaporator can be used as it has been applied in Held *et al.* [23] Due to a lower heat demand and favorable economics, the BASF process is considered in this study (MeOH POX). [5] Therein, methanol reacts with air completely to FA and small amounts of side products (CO_2, CO, and H_2). Water is added to the reactor to avoid explosive mixture compositions and is further added as a solvent in the subsequent absorber, yielding the desired aqueous FA solution.

Table S11: Life cycle inventory of methanol production[23] for the aqueous route via methanol and formaldehyde by partial oxidation of methanol (MeOH POX) with full heat integration per kg of OME_{3-5}.

Flow		Value	Unit
In			
	H_2	-0.250	kg
	CO_2	-1.829	kg
	Air	-1.018	kg
	Electricity	-1.400	MJ
Out			
	Methanol	1.252	kg
	Wastewater	0.720	kg
	Exhaust	1.134	kg
	thereof CO_2	0.113	kg

Table S12: Life cycle inventory of formaldehyde production[23] for the aqueous route via methanol and formaldehyde by partial oxidation of methanol (MeOH POX) with full heat integration per kg of OME_{3-5}.

Flow		Value	Unit
In			
	Methanol	-0.835	kg
	Water	-0.241	kg
	Air	-1.491	kg
	Electricity	-0.043	MJ
Out			
	Formaldehyde, aq (85 wt.-%)	0.824	kg
	Wastewater	0.449	kg
	Exhaust	1.294	kg
	thereof CO_2	0.121	kg

Table S13: Life cycle inventory of OME_{3-5} production[23] for the aqueous route via methanol and formaldehyde by partial oxidation of methanol (MeOH POX) with full heat integration per kg of OME_{3-5}.

Flow		Value	Unit
In			
	Formaldehyde, aq (85 wt.-%)	-0.824	kg
	Methanol	-0.417	kg
	Heat at 143°C	-0.597	MJ
Out			
	OME_{3-5}	1.000	kg
	Wastewater	0.241	kg

Aqueous OME_{3-5} route via methanol and formaldehyde by dehydrogenation of methanol (MeOH DEHY)

The prominent advantage of methanol dehydrogenation (MeOH DEHY) compared to partial oxidation is the significant co-production of H_2 instead of water. This H_2 can be used for the preceding methanol production to lower the overall electricity demand for the entire *Power-to-Fuel* process. However, in contrast to the exothermic BASF process, FA production via dehydrogenation of methanol is an endothermic reaction that requires heating at reactor temperatures of 450-900 °C. [24] Selective and active catalysts have already been identified resulting in a high single-pass FA yield of over 70 %. [24,25] In this study, we assume a copper/zinc/selenium catalyst achieving a methanol

conversion of 69 % and FA selectivity of 90 %, resulting in a yield of 62.1 % at 650 °C reactor temperature. [26] Small amounts of CO and CH_4 are formed as side products. These experimental results have been achieved by methanol dilution with H_2 in the ratio of 1:1 in the reactor feed.

Table S14: Life cycle inventory of methanol production[23] for the aqueous route via methanol and formaldehyde by dehydrogenation of methanol (MeOH DEHY) with full heat integration per kg of OME_{3-5}.

Flow		Value	Unit
In			
	H_2	-0.259	kg
	CO_2	-1.898	kg
	Air	-1.056	kg
	Electricity	-1.400	MJ
Out			
	Methanol	1.299	kg
	Wastewater	0.747	kg
	Exhaust	1.176	kg
	thereof CO_2	0.118	kg

Table S15: Life cycle inventory of formaldehyde production[24–26] for the aqueous route via methanol and formaldehyde by dehydrogenation of methanol (MeOH DEHY) with full heat integration per kg of OME_{3-5}.

Flow		Value	Unit
In			
	Methanol	-1.299	kg
	Water	-0.152	kg
	Air	-2.550	kg
	Electricity	-0.637	MJ
	Heat at 650°C	-2.135	MJ
Out			
	Formaldehyde/Methanol/Water (56/34/10 wt.-%)	1.241	kg
	H_2	0.055	kg
	Exhaust	2.705	kg
	thereof CO_2	0.186	kg

Table S16: Life cycle inventory of OME_{3-5} production[23] for the aqueous route via methanol and formaldehyde by dehydrogenation of methanol (MeOH DEHY) with full heat integration per kg of OME_{3-5}.

Flow		Value	Unit
In			
	Formaldehyde/Methanol/Water (56/34/10 wt.-%)	-1.241	kg
	Heat at 197°C	-3.279	MJ
Out			
	OME_{3-5}	1.000	kg
	Wastewater	0.241	kg

LCA datasets for the background system

Table S17: LCA datasets for the background system.

Flow	Dataset	Region	Reference
Wastewater	treatment of wastewater, average, capacity 1E9l/year	Europe [c]	ecoinvent 3.7 cut-off[27]
Water	Water (desalinated; deionised) ts	EU-28	GaBi [28]
Diesel	Diesel mix at filling station ts	EU-28	GaBi [28]
Electricity	Electricity grid mix (average power plants) ts [a]	EU-28	GaBi [28]
	Electricity from wind power ts [b]	EU-28	GaBi [28]
	Electricity from photovoltaic ts	EU-28	GaBi [28]
	Electricity from solar thermal ts	EU-28	GaBi [28]
	Electricity grid mix ts	DE	GaBi [28]
	Electricity grid mix ts	IT	GaBi [28]
	Electricity grid mix ts	DK	GaBi [28]
	Electricity grid mix ts	AT	GaBi [28]
	Electricity grid mix ts	FI	GaBi [28]
	Electricity grid mix ts	BE	GaBi [28]
	Electricity grid mix ts	CH	GaBi [28]
	Electricity grid mix ts	FR	GaBi [28]
	Electricity grid mix ts	NO	GaBi [28]
Heat below 90°C	steam production, as energy carrier, in chemical industry [a]	Europe	ecoinvent 3.7 cut-off[27]
	Heat pump (COP = 3.28) [b,d]	–	David *et al.* [29]
Heat between 90-250°C	steam production, as energy carrier, in chemical industry [a]	Europe	ecoinvent 3.7 cut-off[27]
	Electrode boiler ($\eta = 0.95$) [b]	–	Müller *et al.* [30]
Heat above 250°C	Thermal energy from natural gas ts [a]	EU-28	GaBi [28]
	Electrode boiler ($\eta = 0.95$) [b]	–	Müller *et al.* [30]
Hydrogen	Hydrogen (steam reforming from natural gas) ts [a]	DE	GaBi [28]
	PEM electrolysis [b]	–	Reuß *et al.* [31]
Carbon dioxide	CO_2 from direct air capture [a]	–	Deutz *et al.* [32]
	CO_2 from ammonia plant [b,e]	–	von der Assen *et al.* [33]

[a] Worst-case scenario.

[b] Best-case scenario.

[c] Without Switzerland.

[d] Averaged coefficient of performance (COP) of heat pumps built beyond 2006 with T_{source} = 9-15°C and $T_{operate}$ = 90°C from David *et al.* [29].

[e] Without electricity consumption for compressing CO_2 to 100 bar for transportation: The OME_{3-5} production routes of this study demand CO_2 at 1 bar and include the CO_2 compression intrinsically in their system boundaries.

S7 Exergy efficiency and specific exergies

The exergy efficiency is calculated as the share of all exergy output flows divided by all exergy input flows:

$$\eta_{\mathrm{Exergy}} = \frac{\dot{E}_{\mathrm{OME}_{3-5}}}{\dot{E}_{\mathrm{H_2}} + \dot{E}_{\dot{\mathrm{Q}}_{\mathrm{in}}} + P_{\mathrm{el}}}.$$

$\dot{E}_{\mathrm{OME}_{3-5}}$, $\dot{E}_{\mathrm{H_2}}$, and $\dot{E}_{\dot{\mathrm{Q}}_{\mathrm{in}}}$ denote the exergy flows associated with the flows of OME_{3-5}, H_2, and the net heat demand $\dot{\mathrm{Q}}_{\mathrm{in}}$, while P_{el} represents the electricity consumption of the OME_{3-5} production system. The net heat demand $\dot{\mathrm{Q}}_{\mathrm{in}}$ is calculated by pinch-based heat integration. Here, CO_2 is not shown as exergy input flow since it brings negligible exergy into the system at 1 bar and 298 K.

Table S18: Specific exergies of considered mass and heat flows. The state of each component is denoted as follows: g for gaseous and l for liquid.

Component	State	Pressure in bar	Temperature in K	Value
Exergy of mass flows in MJ_{Exergy}/kg				
H_2	g	30	298	121.83
CO_2	g	1	298	0.00
Methanol	l	1	298	21.93
Formaldehyde [a]	l	1	298	8.36
Formaldehyde [b]	l	1	298	14.35
Trioxane	l	1	368	17.24
DME	l	10	298	30.21
OME_1	l	1	298	25.01
OME_3	l	1	298	21.42
OME_4	l	1	298	20.78
OME_5	l	1	298	20.23
OME_{3-5} [c]	l	1	298	20.91
OME_{3-5} [d]	l	1	298	20.97
OME_{3-5} [e]	l	1	298	20.80
FA/Methanol/H_2O (56/34/10 wt.-%)	l	1	368	17.27
Exergy of heat flows in MJ_{Exergy}/MJ				
Trioxane production (93°C)			366	0.19
Trioxane production (128°C)			401	0.26
OME_{3-5} production (143°C)			416	0.28
OME_{3-5} production (197°C)			470	0.37
Formaldehyde production (650°C)			923	0.68

[a] 50 wt.-% aq.

[b] 85 wt.-% aq.

[c] Mixture of Burger *et al.*: [34] 42.88 % OME_3, 33.77 % OME_4, 23.35 % OME_5.

[d] Mixture of Held *et al.*: [23] 49.89 % OME_3, 30.69 % OME_4, 19.39 % OME_5.

[e] Mixture of Breitkreuz *et al.*: [19] 33.69 % OME_3, 34.30 % OME_4, 32.01 % OME_5.

S8 Exergy balances

Using the inventories in Section S6 and the specific exergies in Section S7, we can directly compute the exergy flow rates entering and leaving the processes in the considered production routes. The only point that requires additional attention are the heat flows.

For the LCA as well as for computing the overall exergy efficiency of the production routes, we consider full heat integration along the entire production route. This means that any hot and cold stream from each process step (e.g., methanol production, formaldehyde production, $OME_{3\text{-}5}$ production) can be matched with any other cold and hot stream, including streams from other process steps. As such, we only get an overall heat demand for each production route. Since we performed heat integration only by pinch analysis, we just know how much external heating and cooling is required for the entire production route, but we do not know how much heat is transferred within each process step and from one process step to another. While this overall heat demand is sufficient to compute the LCA indicators and the overall exergy efficiency, it does not allow us to obtain exergy balances (or, more specifically, the exergy of heat flows) for each individual process step (e.g., methanol production only).

Nevertheless, we still want to be able to calculate approximate exergy balances for each individual process step in order to visualize the main exergy flows and losses. To do so, we derive an estimate for the heat transfer between the individual process steps as follows. We conduct heat integration by pinch analysis individually for each process step, which gives us an estimate for the required external heating and cooling of each process step as well as the associated temperature levels. We can then approximately match high-enough temperature cooling demand of one process step with lower-temperature heating demand of another process step. This type of heat integration is more restricted than the full heat integration, allowing matches between any two streams considered above. Therefore, it does not yield exactly the same results, but a rough estimate for the heat flows that are exchanged between the process steps.

The resulting exergy balances are given in the following tables.

Anhydrous route via trioxane and OME_1 (TRI+OME_1)

Table S19: Exergy balance of methanol production[15] for the anhydrous route via trioxane and OME_1 (TRI+OME_1). Exergy flows are given for 1 kg of OME_{3-5}.

Exergy flow		Value	Unit
In			
	H_2	-30.40	MJ
	Electricity	-1.27	MJ
Out			
	Methanol	27.89	MJ
	Heat export to OME_1 at 155°C	0.15	MJ
	Heat export to OME_{3-5} at 250/200°C	1.01	MJ
	Loss	2.62	MJ

Table S20: Exergy balance of formaldehyde production[15] for the anhydrous route via trioxane and OME_1 (TRI+OME_1). Exergy flows are given for 1 kg of OME_{3-5}.

Exergy flow		Value	Unit
In			
	Methanol	-18.64	MJ
	Electricity	-0.16	MJ
Out			
	Formaldehyde, aq (50 wt.-%)	12.08	MJ
	Heat export to OME_1 at 200°C	0.92	MJ
	Heat export to trioxane at 200°C	0.74	MJ
	Loss	5.06	MJ

Table S21: Exergy balance of OME_1 production[15] for the anhydrous route via trioxane and OME_1 (TRI+OME_1). Exergy flows are given for 1 kg of OME_{3-5}.

Exergy flow		Value	Unit
In			
	Methanol	-9.25	MJ
	Formaldehyde, aq (50 wt.-%)	-3.29	MJ
	Heat import from methanol at 155°C	-0.15	MJ
	Heat import from formaldehyde at 200°C	-0.92	MJ
	Heat import from OME_{3-5} at 110°C	-0.24	MJ
	Electricity	-0.00	MJ
Out			
	OME_1	12.11	MJ
	Loss	1.74	MJ

Table S22: Exergy balance of trioxane production[16] for the anhydrous route via trioxane and OME_1 (TRI+OME_1). Exergy flows are given for 1 kg of OME_{3-5}.

Exergy flow		Value	Unit
In			
	Formaldehyde, aq (50 wt.-%)	-8.79	MJ
	Heat import from formaldehyde at 200°C	-0.74	MJ
	Heat at 93°C	-2.46	MJ
	Heat at 128°C	-1.33	MJ
	Electricity	-1.04	MJ
Out			
	Trioxane	8.88	MJ
	Loss	5.48	MJ

Table S23: Exergy balance of OME_{3-5} production[16] for the anhydrous route via trioxane and OME_1 (TRI+OME_1). Exergy flows are given for 1 kg of OME_{3-5}.

Exergy flow		Value	Unit
In			
	OME_1	-12.11	MJ
	Trioxane	-8.88	MJ
	Heat import from methanol at 250/200°C	-1.01	MJ
Out			
	OME_{3-5}	20.91	MJ
	Heat export to OME_1 at 110°C	0.24	MJ
	Loss	0.85	MJ

Anhydrous route via trioxane and DME (TRI+DME)

Table S24: Exergy balance of methanol production[15] for the anhydrous route via trioxane and DME (TRI+DME). Exergy flows are given for 1 kg of OME_{3-5}.

Exergy flow		Value	Unit
In			
	H_2	-20.55	MJ
	Electricity	-0.86	MJ
Out			
	Methanol	18.86	MJ
	Heat export to trioxane at 185°C	0.73	MJ
	Loss	1.82	MJ

Table S25: Exergy balance of formaldehyde production[15] for the anhydrous route via trioxane and DME (TRI+DME). Exergy flows are given for 1 kg of OME_{3-5}.

Exergy flow		Value	Unit
In			
	Methanol	-18.86	MJ
	Electricity	-0.16	MJ
Out			
	Formaldehyde, aq (50 wt.-%)	12.22	MJ
	Heat export to trioxane at 200°C	1.02	MJ
	Heat export to OME_{3-5} at 300°C	0.85	MJ
	Loss	4.93	MJ

Table S26: Exergy balance of DME production[20] for the anhydrous route via trioxane and DME (TRI+DME). Exergy flows are given for 1 kg of OME_{3-5}.

Exergy flow		Value	Unit
In			
	H_2	-9.24	MJ
	Electricity	-0.41	MJ
Out			
	DME	8.58	MJ
	Heat export to trioxane at 195°C	0.16	MJ
	Loss	0.91	MJ

Table S27: Exergy balance of trioxane production[16] for the anhydrous route via trioxane and DME (TRI+DME). Exergy flows are given for 1 kg of OME_{3-5}.

Exergy flow		Value	Unit
In			
	Formaldehyde, aq (50 wt.-%)	-12.22	MJ
	Heat import from methanol at 185°C	-0.73	MJ
	Heat import from formaldehyde at 200°C	-1.02	MJ
	Heat import from DME at 195°C	-0.16	MJ
	Heat at 93°C	-2.90	MJ
	Heat at 128°C	-2.51	MJ
	Electricity	-1.44	MJ
Out			
	Trioxane	12.34	MJ
	Loss	8.64	MJ

Table S28: Exergy balance of OME_{3-5} production[19] for the anhydrous route via trioxane and DME (TRI+DME). Exergy flows are given for 1 kg of OME_{3-5}.

Exergy flow		Value	Unit
In			
	DME	-8.58	MJ
	Trioxane	-12.34	MJ
	Heat import from formaldehyde at 300°C	-0.85	MJ
Out			
	OME_{3-5}	20.80	MJ
	Loss	0.97	MJ

Aqueous route via methanol and formaldehyde by partial oxidation of methanol (MeOH POX)

Table S29: Exergy balance of methanol production[23] for the aqueous route via methanol and formaldehyde by partial oxidation of methanol (MeOH POX). Exergy flows are given for 1 kg of OME_{3-5}.

Exergy flow		Value	Unit
In			
	H_2	-30.47	MJ
	Electricity	-1.40	MJ
Out			
	Methanol	27.45	MJ
	Heat export to OME_{3-5} at 650/230°C	1.54	MJ
	Loss	2.88	MJ

Table S30: Exergy balance of formaldehyde production[23] for the aqueous route via methanol and formaldehyde by partial oxidation of methanol (MeOH POX). Exergy flows are given for 1 kg of OME_{3-5}.

Exergy flow		Value	Unit
In			
	Methanol	-18.31	MJ
	Electricity	-0.04	MJ
Out			
	Formaldehyde, aq (85 wt.-%)	11.83	MJ
	Heat export to OME_{3-5} at 650/200°C	2.79	MJ
	Loss	3.73	MJ

Table S31: Exergy balance of OME_{3-5} production[23] for the aqueous route via methanol and formaldehyde by partial oxidation of methanol (MeOH POX). Exergy flows are given for 1 kg of OME_{3-5}.

Exergy flow		Value	Unit
In			
	Formaldehyde, aq (85 wt.-%)	-11.83	MJ
	Methanol	-9.14	MJ
	Heat import from methanol at 650/230°C	-1.54	MJ
	Heat import from formaldehyde at 650/200°C	-2.79	MJ
	Heat at 143°C	-0.17	MJ
Out			
	OME_{3-5}	20.97	MJ
	Loss	4.50	MJ

Aqueous route via methanol and formaldehyde by dehydrogenation of methanol (MeOH DEHY)

Table S32: Exergy balance of methanol production[23] for the aqueous route via methanol and formaldehyde by dehydrogenation of methanol (MeOH DEHY). Exergy flows are given for 1 kg of OME_{3-5}.

Exergy flow		Value	Unit
In			
	H_2	-24.96	MJ
	H_2 recycle from formaldehyde	-6.65	MJ
	Electricity	-1.40	MJ
Out			
	Methanol	28.48	MJ
	Heat export to OME_{3-5} at 650/200°C	1.93	MJ
	Loss	2.60	MJ

Table S33: Exergy balance of formaldehyde production[24–26] for the aqueous route via methanol and formaldehyde by dehydrogenation of methanol (MeOH DEHY). Exergy flows are given for 1 kg of OME_{3-5}.

Exergy flow		Value	Unit
In			
	Methanol	-28.48	MJ
	Heat at 650°C	-1.45	MJ
	Electricity	-0.64	MJ
Out			
	Formaldehyde/Methanol/Water (56/34/10 wt.-%)	21.44	MJ
	H_2 recycle to methanol	6.65	MJ
	Heat export to OME_{3-5} at 200°C	0.67	MJ
	Loss	1.81	MJ

Table S34: Exergy balance of OME_{3-5} production[23] for the aqueous route via methanol and formaldehyde by dehydrogenation of methanol (MeOH DEHY). Exergy flows are given for 1 kg of OME_{3-5}.

Exergy flow		Value	Unit
In			
	Formaldehyde/Methanol/Water (56/34/10 wt.-%)	-21.44	MJ
	Heat import from methanol at 650/200°C	-1.93	MJ
	Heat import from formaldehyde at 200°C	-0.67	MJ
	Heat at 197°C	-1.20	MJ
Out			
	OME_{3-5}	20.97	MJ
	Loss	4.27	MJ

S9 Emission measurement

Table S35: Specifications of the single-cylinder engine.

Feature	Unit	Value
Bore	mm	75
Stroke	mm	88.3
Displacement	Liter	0.39
Compression ratio	-	15:1
Swirl number	-	1.25
Max. injection pressure	bar	2000
Max. boost pressure (abs.)	bar	4
Peak firing pressure	bar	220
Max. engine speed	1/min	5500
Piston bowl geometry	-	Aluminum piston with ω-shaped reentrant

Table S36: Measuring devices for species concentration, air mass flow, and fuel mass flow.

Emission	Measuring principle	Device
Soot	Filter paper method	AVL 415s
Particle number and size	Differential electrical mobility separation	TSI Engine exhaust particle sizer 3090
NO_x	Chemiluminescence detector	EcoPysics CLD 700 EL
HC as C_3H_8 equivalent	Flame ionization detector	Rosemount – NGA 2000
CO & CO_2	Non dispersive infrared	Rosemount – NGA 2000
O_2	Paramagnetic detector	Rosemount – NGA 2000
Formaldehyde & CH_4	FTIR	FEV EmissionRate
Fuel mass flow	Coriolis	FEV FuelRate
Air mass flow	Ultrasonic	FEV AirRate

Table S37: Data for the vehicle, engine, and after-treatment system model.

Parameter name	Value	unit
Vehicle mass	1590	kg
Gears	7	-
1st gear ratio	4	-
2nd gear ratio	2.1	-
3rd gear ratio	1.38	-
4th gear ratio	1	-
5th gear ratio	0.78	-
6th gear ratio	0.65	-
7th gear ratio	0.52	-
Final drive ratio	2.93	-
Rolling resistance curve	$0.04v^2$-$0.32v$+175	N
Drive train efficiency	0.95	-
Wheel diameter	61	cm
Engine displacement	1600	cm^3
Inertia of turbine and compressor wheel	$5x10^{-5}$	kg m^2
DPF volume	3000	cm^3
SCR volume	3600	cm^3
DOC volume	1300	cm^3
Initial temp. of after-treatment system	300	K

Table S38: Variation domain for the global design of experiment (DOE) approach.

Variation parameter	Range	Distribution	Constraints
OME_{3-5} content in fuel	0-100%	Predefined	0%, 35 vol.%, 100%
Engine speed	1000 – 2750 rpm	In steps of 250 rpm	No constraint
Imep of the high pressure cycle	1.5 – 19.5 bar	In steps of 2 bar,	Constrained by full load at low engine speeds
Center of combustion	5 – 20 °CAaTDC	Random	±5 °CAaTDC from basis value for corresponding load point
Rail pressure	200 – 2000 bar	Random	±300 bar from basis value for corresponding load point
Pilot energizing time	180 - 300 us	Random	No constraint
Pilot offset rel. to main Inj.	800 – 3000 µs	Random	Constrained to -30 °CAaTDC
Boost pressure	1 – 3 bar	Random	±0.3 bar from basis value for corresponding load point
EGR rate	0-70%,	Random	Constrained by λ >1.1 for diesel and by λ >0.9 for pure OME_{3-5}

Table S39: The cumulated tailpipe emissions of fossil diesel, diesel-OME_{3-5} blends, and pure OME_{3-5} as well as the energy consumption of the passenger car.

Fuel	NO_x emissions	Soot emissions	CO_2 emissions	Energy consumption
–	mg/km	mg/km	g/km	MJ/km
Fossil diesel	58	0.56	115	1.57
20 vol.-% OME_{3-5} in fossil diesel	40	0.40	117	
35 vol.-% OME_{3-5} in fossil diesel	31	0.23	119	
50 vol.-% OME_{3-5} in fossil diesel	25	0.08	121	
Pure OME_{3-5}	25	0.00	131	

S10 Flowsheet of the OME_{3-5} production via methanol and formaldehyde by dehydrogenation of methanol (MeOH DEHY)

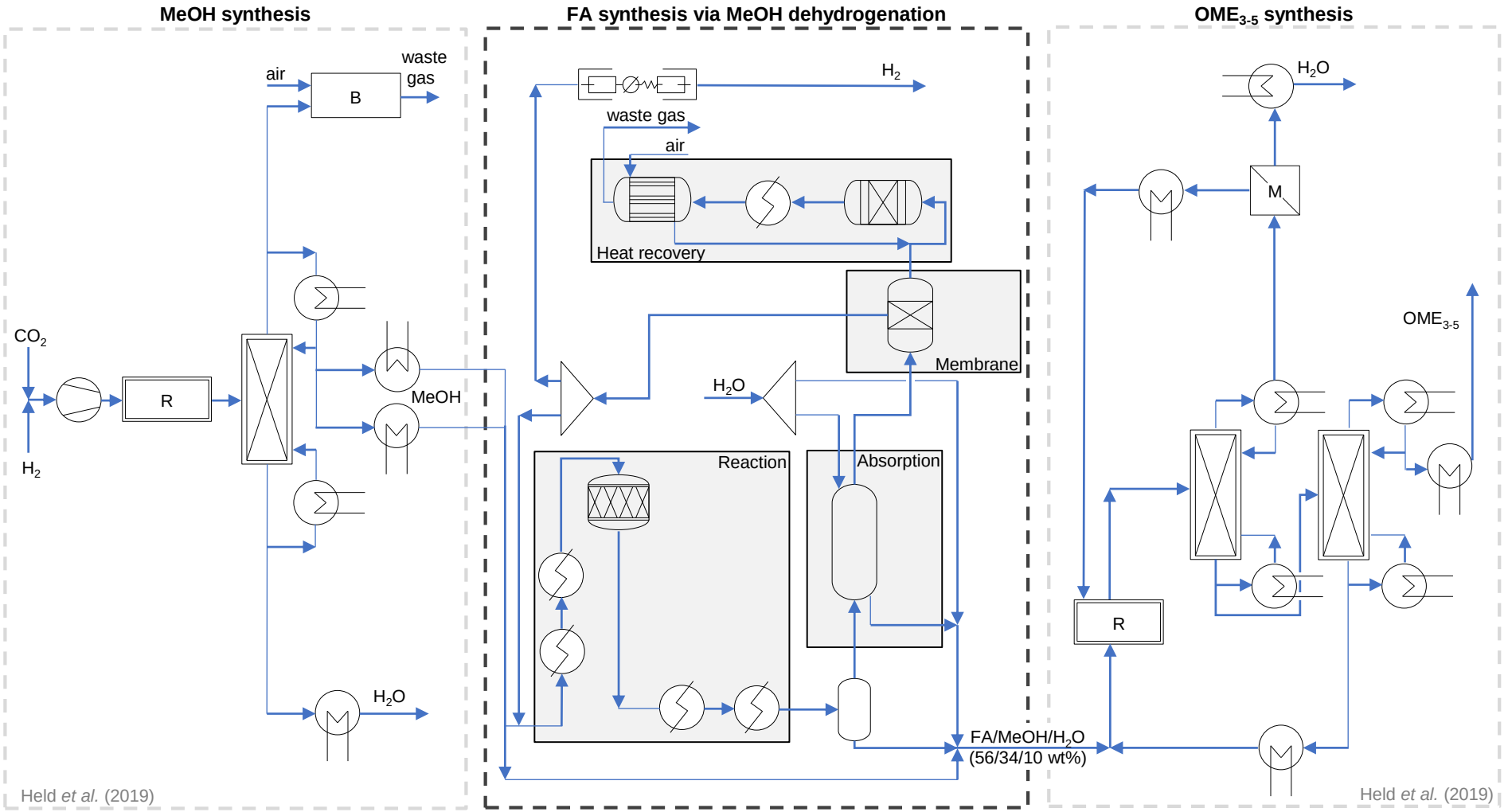

Figure S7: Flowsheet of the OME_{3-5} route via methanol and formaldehyde by dehydrogenation of methanol (MeOH DEHY route). The simplified process flowsheets for methanol and OME_{3-5} synthesis are taken from Held et al., [23] while the formaldehyde synthesis via dehydrogenation of methanol has been developed in this study.

S11 Calculations for the analysis of blending OME_{3-5} gradually into the EU fleet of diesel passenger cars

***"Blend for all"*: Blending OME_{3-5} and fossil diesel for the entire fleet**

We estimate the current annual mileage of the diesel passenger car fleet in the European Union (EU) ($mileage^{\mathrm{EU,annual}}_{\mathrm{diesel\ passenger\ cars}}$) as the product of the amount of diesel passenger cars in the EU ($n^{\mathrm{EU}}_{\mathrm{diesel\ passenger\ cars}}$) and the average annual mileage per passenger car in the EU ($mileage^{\mathrm{EU,annual,average}}_{\mathrm{passenger\ car}}$):

$$mileage^{\mathrm{EU,annual}}_{\mathrm{diesel\ passenger\ cars}} = n^{\mathrm{EU}}_{\mathrm{diesel\ passenger\ cars}} \cdot mileage^{\mathrm{EU,annual,average}}_{\mathrm{passenger\ car}} . \quad \text{(Eq. 1)}$$

The annual mileage of the EU fleet of diesel passenger cars results in 1.34×10^{12} km with 95.7 million diesel passenger cars [35] and an estimated average annual mileage of 14,000 km in the EU. [36]

The transportation demand is proportional to the total enthalpy of combustion of the diesel-OME_{3-5} blend (E_{blend}), assuming equal energy consumptions ($e_{\mathrm{diesel\ passenger\ car}}$) for all diesel passenger cars:

$$E_{\mathrm{blend}} = mileage^{\mathrm{EU,annual}}_{\mathrm{diesel\ passenger\ cars}} \cdot e_{\mathrm{diesel\ passenger\ car}} . \quad \text{(Eq. 2)}$$

The mass of produced OME_{3-5} is determined by the amount of available electricity ($W_{\mathrm{el,additional}}$) and the specific electricity consumption to produce 1 kg of OME_{3-5} ($w_{\mathrm{el,OME_{3-5}}}$):

$$m_{\mathrm{OME_{3-5}}} = \frac{W_{\mathrm{el,additional}}}{w_{\mathrm{el,OME_{3-5}}}} . \quad \text{(Eq. 3)}$$

The enthalpy of combustion of OME_{3-5} ($E_{\mathrm{OME_{3-5}}}$) is proportional to the mass of produced OME_{3-5} and the specific lower heating value of OME_{3-5} ($LHV_{\mathrm{OME_{3-5}}}$):

$$E_{\mathrm{OME_{3-5}}} = m_{\mathrm{OME_{3-5}}} \cdot LHV_{\mathrm{OME_{3-5}}} . \quad \text{(Eq. 4)}$$

The sum of the enthalpies of combustion of OME_{3-5} and diesel (E_{diesel}) equals the total enthalpy of combustion of the diesel-OME_{3-5} blend (Figure S8), assuming ideal mixing and equal energy consumptions per km. Therefore, the enthalpy of combustion of diesel can be calculated as follows:

$$E_{\mathrm{diesel}} = E_{\mathrm{blend}} - E_{\mathrm{OME_{3-5}}} . \quad \text{(Eq. 5)}$$

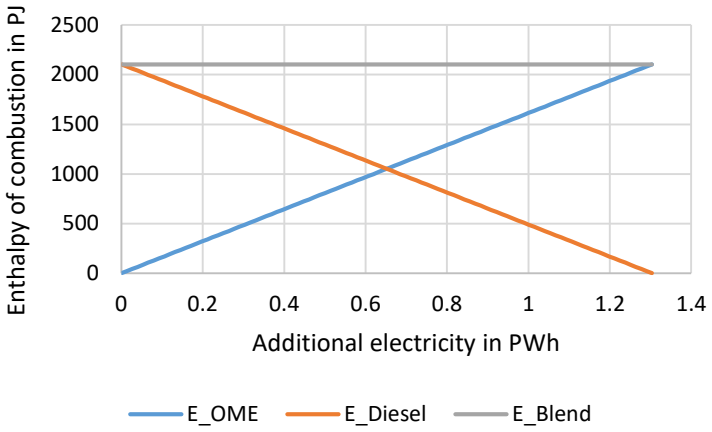

Figure S8: Energy balance of the enthalpies of combustion: The sum of both enthalpies of combustion of OME_{3-5} and diesel equals the total enthalpy of combustion of the blend.

The mass of produced diesel (m_{diesel}) is proportional to the enthalpy of combustion of diesel and the specific lower heating value of diesel (LHV_{diesel}):

$$m_{\mathrm{diesel}} = \frac{E_{\mathrm{diesel}}}{LHV_{\mathrm{diesel}}} . \qquad \text{(Eq. 6)}$$

The total blend mass (m_{blend}) is the sum of the masses of produced OME_{3-5} and diesel:

$$m_{\mathrm{blend}} = m_{\mathrm{OME}_{3-5}} + m_{\mathrm{diesel}} . \qquad \text{(Eq. 7)}$$

The total blend mass increases with increasing mass of produced OME_{3-5} (Figure S9). This is due to the lower specific lower heating value of OME_{3-5} compared to that of fossil diesel: Substituting 1.0 kg of fossil diesel requires 2.2 kg of OME_{3-5} to provide the same amount of enthalpy of combustion, assuming a constant energy consumption of the passenger car for both fuels. Note that we neglect the effect of increasing fuel mass on the mileage.

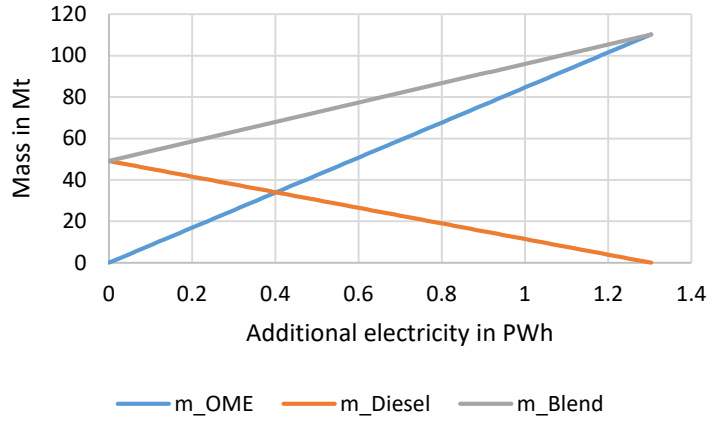

Figure S9: The total blend mass, OME_{3-5} mass and fossil diesel mass as functions of the additionally available electricity.

The mass fractions of OME$_{3\text{-}5}$ ($y_{\mathrm{OME}_{3-5},\mathrm{blend}}$) and diesel ($y_{\mathrm{diesel},\mathrm{blend}}$) within the blend are calculated as follows:

$$y_{\mathrm{OME}_{3-5},\mathrm{blend}} = \frac{m_{\mathrm{OME}_{3-5}}}{m_{\mathrm{blend}}}, \qquad \text{(Eq. 8)}$$

$$y_{\mathrm{diesel},\mathrm{blend}} = 1 - y_{\mathrm{OME}_{3-5},\mathrm{blend}}\,. \qquad \text{(Eq. 9)}$$

As stated above, the total blend mass increases with increasing mass of produced OME$_{3\text{-}5}$. This results in nonlinear functions of additional electricity for both mass fractions (Figure S10). The mass fraction of OME$_{3\text{-}5}$, which equals the specific blending ratio of OME$_{3\text{-}5}$, is a concave function of the amount of additionally available electricity. A blending component with a higher lower heating value than fossil diesel would instead result in a convex function, while a blending component with the same lower heating value as fossil diesel would result in a linear function.

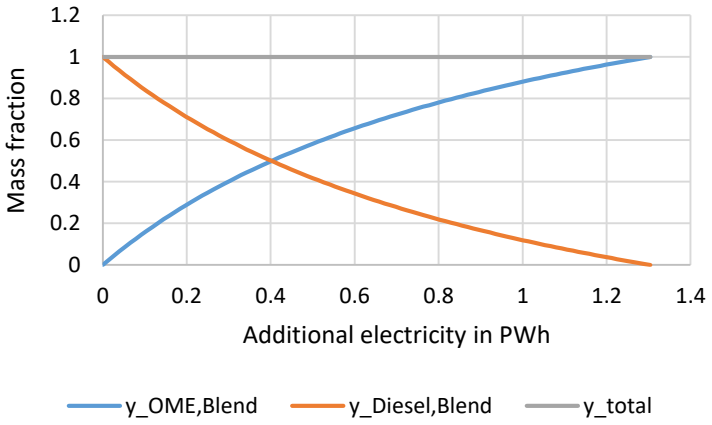

Figure S10: The mass fractions of OME$_{3\text{-}5}$ and diesel within the blend as functions of the additionally available electricity.

The specific blending ratio of OME$_{3\text{-}5}$ (BR_{mass}) equals the mass fraction of OME$_{3\text{-}5}$ within the blend:

$$BR_{\mathrm{mass}} = \frac{m_{\mathrm{OME}_{3-5}}}{m_{\mathrm{blend}}} = y_{\mathrm{OME}_{3-5},\mathrm{blend}}\,. \qquad \text{(Eq. 10)}$$

The volumetric blending ratio of OME$_{3\text{-}5}$ ($BR_{\mathrm{volumetric}}$) is the ratio of the OME$_{3\text{-}5}$ volume ($V_{\mathrm{OME}_{3-5}}$) and the total blend volume. The total blend volume is the sum of the OME$_{3\text{-}5}$ and the diesel volume (V_{diesel}). Both the OME$_{3\text{-}5}$ and diesel volume are proportional to the ratios of their masses and densities ($\rho_{\mathrm{OME}_{3-5}}$ and ρ_{diesel}):

$$BR_{\mathrm{volumetric}} = \frac{V_{\mathrm{OME}_{3-5}}}{V_{\mathrm{OME}_{3-5}} + V_{\mathrm{diesel}}} = \frac{m_{\mathrm{OME}_{3-5}}/\rho_{\mathrm{OME}_{3-5}}}{m_{\mathrm{OME}_{3-5}}/\rho_{\mathrm{OME}_{3-5}} + m_{\mathrm{diesel}}/\rho_{\mathrm{diesel}}}\,. \qquad \text{(Eq. 11)}$$

The lower heating value of the blend (LHV_{blend}) is obtained by the sum of the products of each component's mass fraction and specific lower heating value:

$$LHV_{\mathrm{blend}} = \sum_i y_{\mathrm{i,blend}} \cdot LHV_i = y_{\mathrm{OME_{3-5},blend}} \cdot LHV_{\mathrm{OME_{3-5}}} + y_{\mathrm{diesel,blend}} \cdot LHV_{\mathrm{diesel}} \,. \quad \text{(Eq. 12)}$$

The lower heating value of the diesel-$OME_{3\text{-}5}$ blend is a convex, monotonically decreasing function of the amount of additionally available electricity and ranges in the interval of both pure fuels' lower heating values (Figure S11).

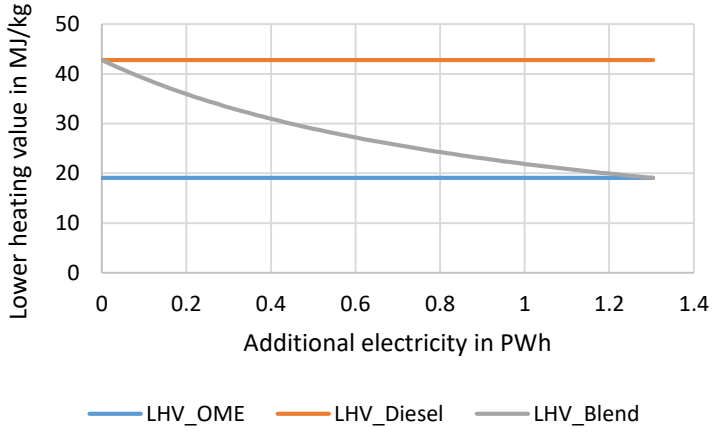

Figure S11: The lower heating values of pure $OME_{3\text{-}5}$ and pure fossil diesel as well as the lower heating value of diesel-$OME_{3\text{-}5}$ blends as function of the additionally available electricity.

The environmental impact (EI) of the fleet for *"blend for all"* ($EI_{\mathrm{Fleet}}^{\mathrm{Blend\ for\ all}}$) follows from emission measurements for each volumetric blending ratio (cf. Section 3.2 and S9).

***"Pure for few"*: Using pure $OME_{3\text{-}5}$ and pure fossil diesel separately in the fleet**

For *"pure for few,"* we calculate the mileage of diesel passenger cars with pure $OME_{3\text{-}5}$ as the fraction of the enthalpy of combustion of $OME_{3\text{-}5}$ ($E_{\mathrm{OME_{3-5}}}$) and the energy consumption of diesel passenger cars ($e_{\mathrm{diesel\ passenger\ car}}$). The enthalpy of combustion of $OME_{3\text{-}5}$ follows from the amount of produced $OME_{3\text{-}5}$ depending on the available electricity for $OME_{3\text{-}5}$ production (Eq. 3 and 4).

$$mileage_{\mathrm{OME_{3-5}}} = \frac{E_{\mathrm{OME_{3-5}}}}{e_{\mathrm{diesel\ passenger\ car}}} \,. \quad \text{(Eq. 13)}$$

We estimate the mileage of diesel passenger cars with pure fossil diesel by subtracting the mileage of diesel passenger cars with pure $OME_{3\text{-}5}$ from the current annual mileage of the EU fleet of diesel passenger cars (Eq. 1):

$$mileage_{\mathrm{diesel}} = mileage_{\mathrm{diesel\ passenger\ cars}}^{\mathrm{EU,annual}} - mileage_{\mathrm{OME_{3-5}}} \,. \quad \text{(Eq. 14)}$$

The mileage shares of pure OME_{3-5} and pure fossil diesel can then be calculated as follows:

$$share_{\mathrm{OME_{3-5}}}^{\mathrm{mileage}} = \frac{mileage_{\mathrm{OME_{3-5}}}}{mileage_{\text{diesel passenger cars}}^{\mathrm{EU,annual}}}, \quad \text{(Eq. 15)}$$

$$share_{\mathrm{diesel}}^{\mathrm{mileage}} = \frac{mileage_{\mathrm{diesel}}}{mileage_{\text{diesel passenger cars}}^{\mathrm{EU,annual}}} = 1 - share_{\mathrm{OME_{3-5}}}^{\mathrm{mileage}}. \quad \text{(Eq. 16)}$$

The environmental impact (EI) of the fleet for *"pure for few"* ($EI_{\mathrm{Fleet}}^{\mathrm{Pure\ for\ few}}$) is the sum of the products of the mileage shares and the environmental impacts of driving a diesel passenger car with pure OME_{3-5} ($EI_{\mathrm{OME_{3-5},pure}}$) and pure fossil diesel ($EI_{\mathrm{diesel,pure}}$), respectively. The environmental impacts of pure OME_{3-5} and pure fossil diesel stem from emission measurements (cf. Section 3.2 and S9).

$$EI_{\mathrm{Fleet}}^{\mathrm{Pure\ for\ few}} = share_{\mathrm{OME_{3-5}}}^{\mathrm{mileage}} \cdot EI_{\mathrm{OME_{3-5},pure}} + share_{\mathrm{diesel}}^{\mathrm{mileage}} \cdot EI_{\mathrm{diesel,pure}} \quad \text{(Eq. 17)}$$

S12 Contribution analyses of the well-to-wheel environmental impacts for *"blend for all"* as function of the additionally available electricity for OME_{3-5} production

In this section, we present contribution analyses of the environmental impacts for the case *"blend for all"* and various electricity supplies as function of the additionally available electricity for OME_{3-5} production.

Note that respiratory effects and photochemical ozone formation are significantly higher with electricity from photovoltaic (Figure S14) than with electricity from wind power (Figure S17). The considered LCA datasets of the LCA database GaBi assume manufacturing of photovoltaic modules mostly in China, whereas most wind turbine components are assumed to be produced in Europe. In contrast to Europe, China's electricity mix has a higher proportion of coal-fired power plants with higher specific NO_x, sulphur dioxide, and particulate matter emissions, increasing both environmental impacts strongly. [28]

Furthermore, photochemical ozone formation shows a minimum between 0 and 0.5 PWh of additional electricity for Switzerland, France, and photovoltaic (Figure S12-S14). For these electricity supplies, emissions from electricity production overcompensate the nonlinear reduction of NO_x emissions during fuel combustion at these minima.

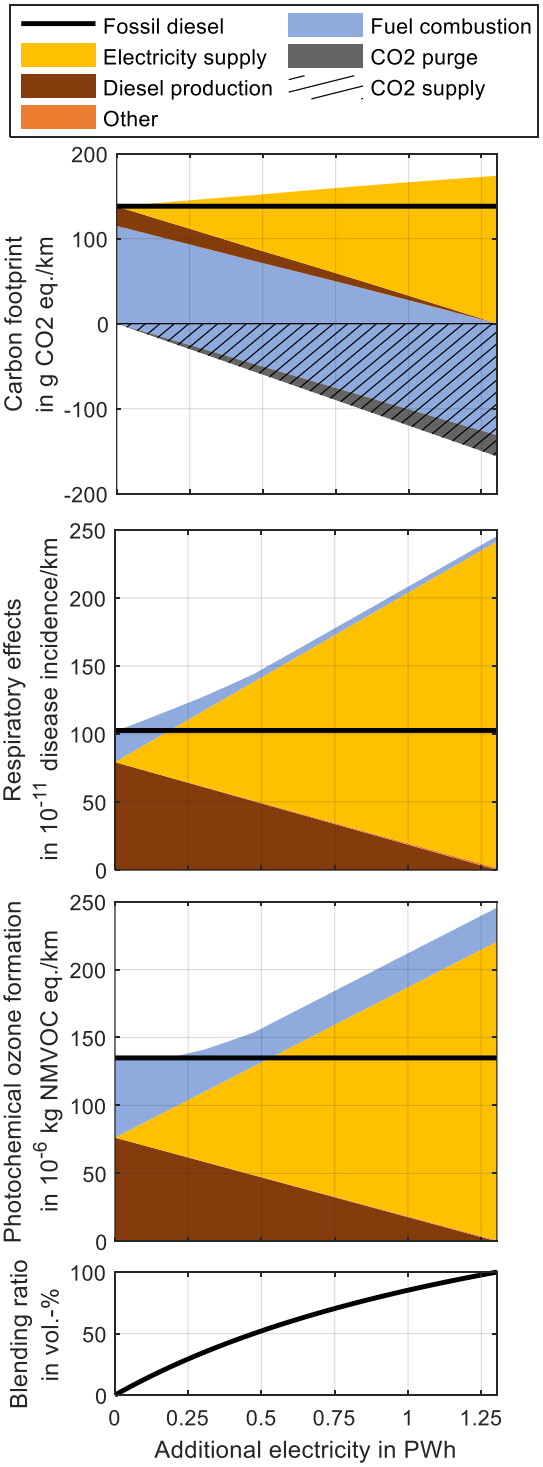

*Figure S12: Well-to-wheel carbon footprint, respiratory effects, photochemical ozone formation, and the volumetric blending ratio as functions of additionally available electricity for $OME_{3\text{-}5}$ production. Results are shown for the electricity supply of **Switzerland (CH)**. The well-to-wheel impacts include emissions along the entire life cycle of diesel-$OME_{3\text{-}5}$ blends. The black bold line represents the environmental impacts of the conventional fossil diesel system. CO_2 is supplied by an ammonia plant.*

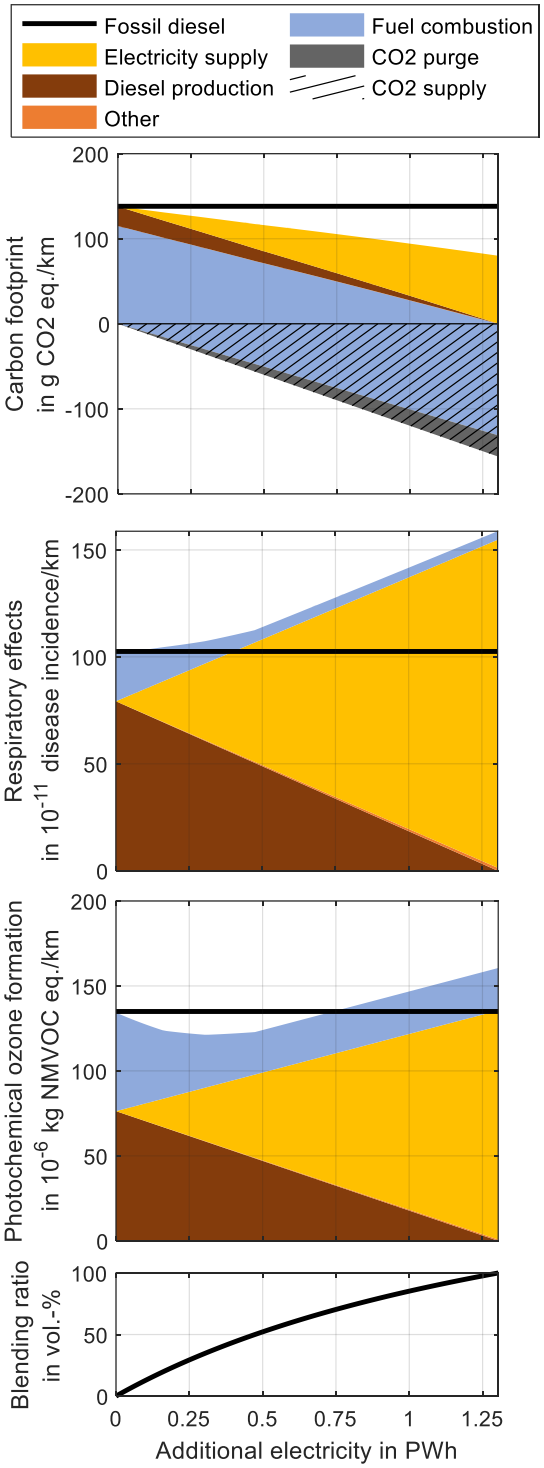

*Figure S13: Well-to-wheel carbon footprint, respiratory effects, photochemical ozone formation, and the volumetric blending ratio as functions of additionally available electricity for $OME_{3\text{-}5}$ production. Results are shown for the electricity supply of **France (FR)**. The well-to-wheel impacts include emissions along the entire life cycle of diesel-$OME_{3\text{-}5}$ blends. The black bold line represents the environmental impacts of the conventional fossil diesel system. CO_2 is supplied by an ammonia plant.*

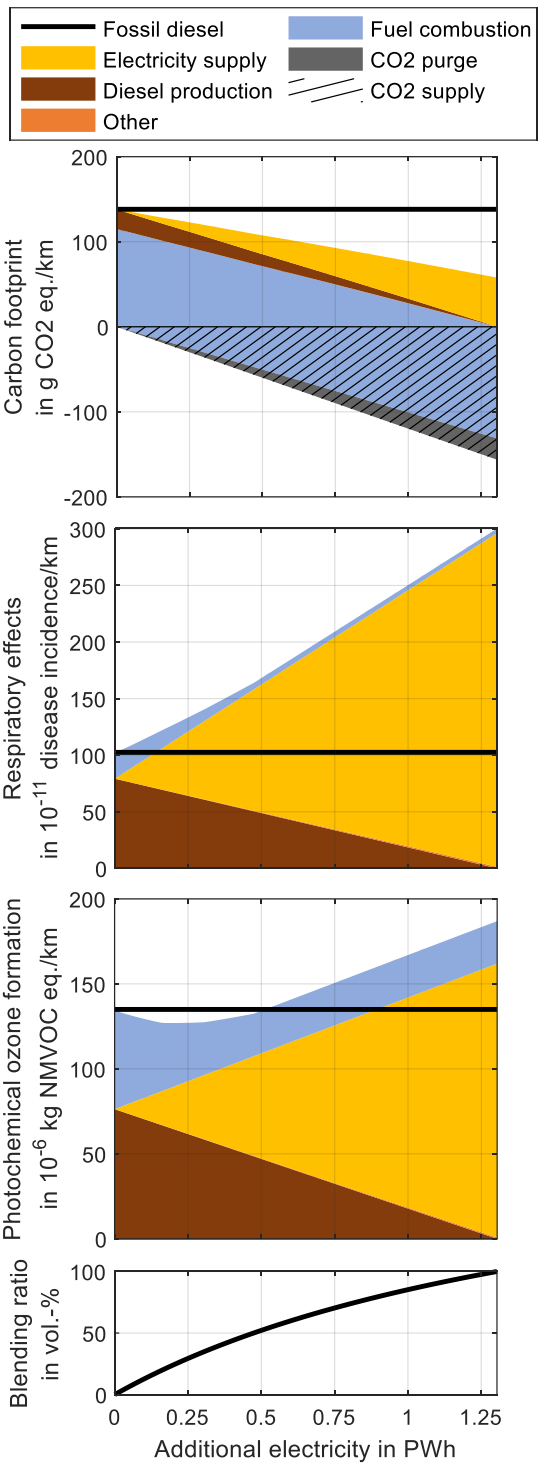

*Figure S14: Well-to-wheel carbon footprint, respiratory effects, photochemical ozone formation, and the volumetric blending ratio as functions of additionally available electricity for $OME_{3\text{-}5}$ production. Results are shown for the electricity supply by **photovoltaic (PV)**. The well-to-wheel impacts include emissions along the entire life cycle of diesel-$OME_{3\text{-}5}$ blends. The black bold line represents the environmental impacts of the conventional fossil diesel system. CO_2 is supplied by an ammonia plant.*

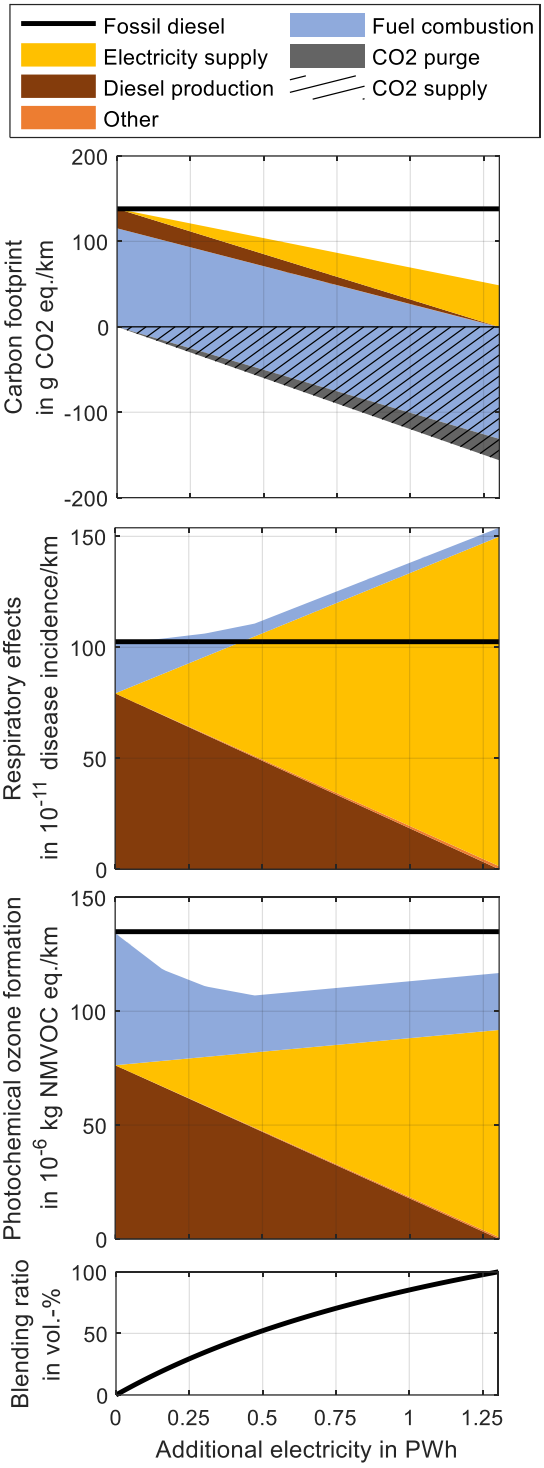

*Figure S15: Well-to-wheel carbon footprint, respiratory effects, photochemical ozone formation, and the volumetric blending ratio as functions of additionally available electricity for $OME_{3\text{-}5}$ production. Results are shown for the electricity supply by **solar-thermal (ST) energy**. The well-to-wheel impacts include emissions along the entire life cycle of diesel-$OME_{3\text{-}5}$ blends. The black bold line represents the environmental impacts of the conventional fossil diesel system. CO_2 is supplied by an ammonia plant.*

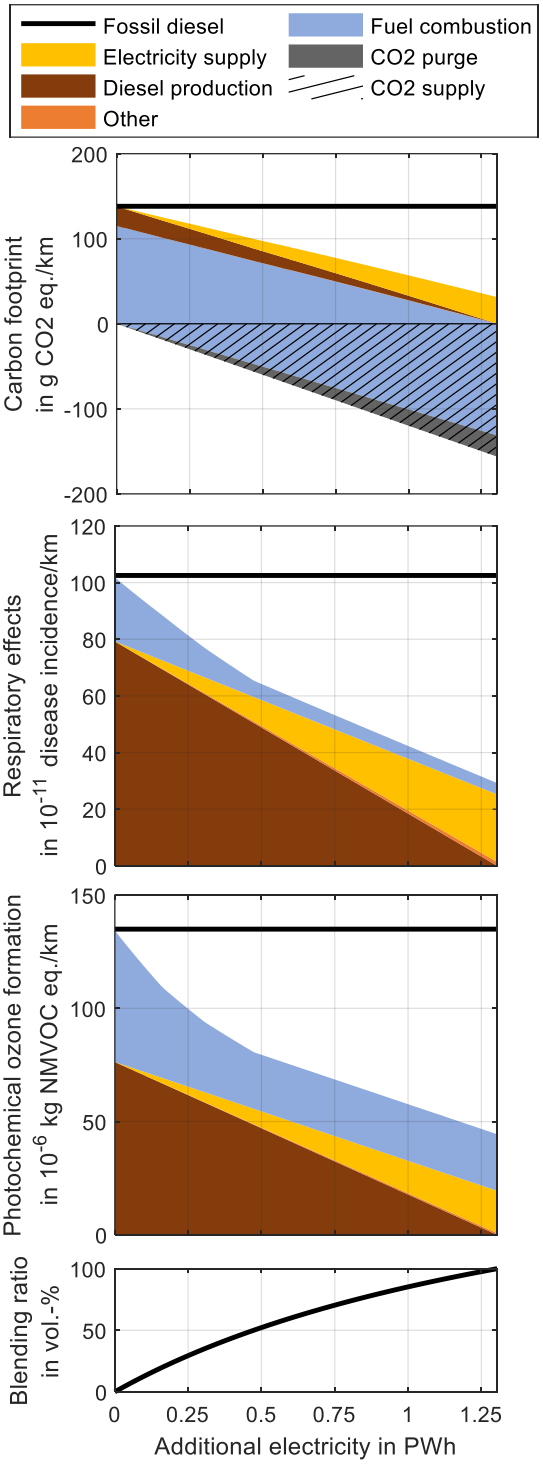

*Figure S16: Well-to-wheel carbon footprint, respiratory effects, photochemical ozone formation, and the volumetric blending ratio as functions of additionally available electricity for $OME_{3\text{-}5}$ production. Results are shown for the electricity supply of **Norway (NO)**. The well-to-wheel impacts include emissions along the entire life cycle of diesel-$OME_{3\text{-}5}$ blends. The black bold line represents the environmental impacts of the conventional fossil diesel system. CO_2 is supplied by an ammonia plant.*

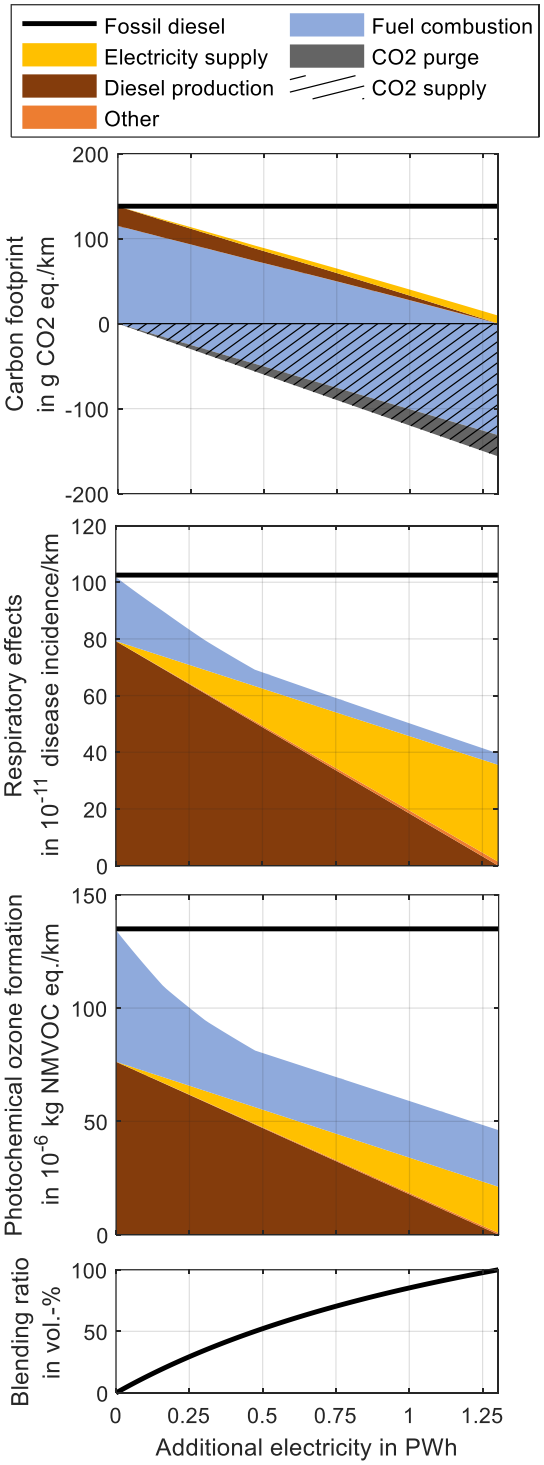

*Figure S17: Well-to-wheel carbon footprint, respiratory effects, photochemical ozone formation, and the volumetric blending ratio as functions of additionally available electricity for $OME_{3\text{-}5}$ production. Results are shown for the electricity supply by **wind power**. The well-to-wheel impacts include emissions along the entire life cycle of diesel-$OME_{3\text{-}5}$ blends. The black bold line represents the environmental impacts of the conventional fossil diesel system. CO_2 is supplied by an ammonia plant.*

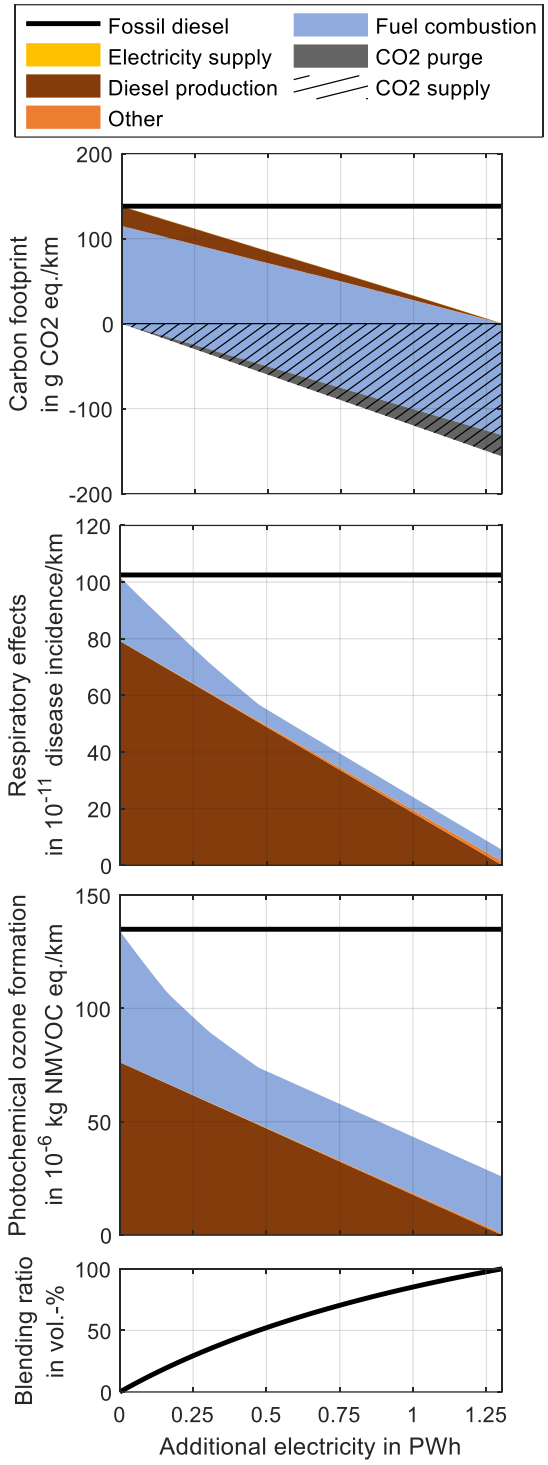

Figure S18: Well-to-wheel carbon footprint, respiratory effects, photochemical ozone formation, and the volumetric blending ratio as functions of additionally available electricity for $OME_{3\text{-}5}$ production. Results are shown for the ***theoretical limit of a burden-free electricity supply****. The well-to-wheel impacts include emissions along the entire life cycle of diesel-$OME_{3\text{-}5}$ blends. The black bold line represents the environmental impacts of the conventional fossil diesel system. CO_2 is supplied by an ammonia plant.*

S13 References

1. G. Maurer, *AIChE J.*, 1986, **32**(6), 932.
2. N. Schmitz, F. Homberg, J. Berje, J. Burger and H. Hasse, *Ind. Eng. Chem. Res.*, 2015, **54**(25), 6409.
3. J. Burger, M. Siegert, E. Ströfer and H. Hasse, *Fuel*, 2010, **89**(11), 3315.
4. N. Schmitz, E. Ströfer, J. Burger and H. Hasse, *Ind. Eng. Chem. Res.*, 2017, **56**(40), 11519.
5. G. Reuss, W. Disteldorf, A. O. Gamer and A. Hilt in *Ullmann's Encyclopedia of Industrial Chemistry*, Wiley-VCH Verlag GmbH & Co. KGaA, Weinheim, Germany, 2000, p 377.
6. T. Grützner, H. Hasse, N. Lang, M. Siegert and E. Ströfer, *Chemical Engineering Science*, 2007, **62**(18-20), 5613.
7. J. Mahieux, *Hydrocarbon Process., Int. Ed.*, 1969, **48**, 163.
8. J.-O. Weidert, J. Burger, M. Renner, S. Blagov and H. Hasse, *Ind. Eng. Chem. Res.*, 2017, **56**(2), 575.
9. J. Burger, E. Ströfer and H. Hasse, *Ind. Eng. Chem. Res.*, 2012, **51**(39), 12751.
10. L. Wang, W.-T. Wu, T. Chen, Q. Chen and M.-Y. He, *Chemical Engineering Communications*, 2014, **201**(5), 709.
11. Q. Wu, M. Wang, Y. Hao, H. Li, Y. Zhao and Q. Jiao, *Ind. Eng. Chem. Res.*, 2014, **53**(42), 16254.
12. J. Wu, H. Zhu, Z. Wu, Z. Qin, L. Yan, B. Du, W. Fan and J. Wang, *Green Chem.*, 2015, **17**(4), 2353.
13. Y. Wu, Z. Li and C. Xia, *Ind. Eng. Chem. Res.*, 2016, **55**(7), 1859.
14. L. Lautenschütz, D. Oestreich, P. Haltenort, U. Arnold, E. Dinjus and J. Sauer, *Fuel Processing Technology*, 2017, **165**, 27.
15. D. Bongartz, J. Burre and A. Mitsos, *Ind. Eng. Chem. Res.*, 2019, **58**(12), 4881.
16. J. Burre, D. Bongartz and A. Mitsos, *Ind. Eng. Chem. Res.*, 2019, **58**(14), 5567.
17. Z. Azizi, M. Rezaeimanesh, T. Tohidian and M. R. Rahimpour, *Chemical Engineering and Processing - Process Intensification*, 2014, **82**, 150.
18. W.-J. Shen, K.-W. Jun, H.-S. Choi and K.-W. Lee, *Korean J. Chem. Eng.*, 2000, **17**(2), 210.
19. C. F. Breitkreuz, N. Schmitz, E. Ströfer, J. Burger and H. Hasse, *Chemie Ingenieur Technik*, 2018, **90**(10), 1489.
20. D. Bongartz, L. Doré, K. Eichler, T. Grube, B. Heuser, L. E. Hombach, M. Robinius, S. Pischinger, D. Stolten, G. Walther and A. Mitsos, *Applied Energy*, 2018, **231**, 757.
21. H. Hasse, I. Hahnenstein and G. Maurer, *AIChE J.*, 1990, **36**(12), 1807.
22. N. Schmitz, J. Burger and H. Hasse, *Ind. Eng. Chem. Res.*, 2015, **54**(50), 12553.
23. M. Held, Y. Tönges, D. Pélerin, M. Härtl, G. Wachtmeister and J. Burger, *Energy Environ. Sci.*, 2019, **12**(3), 1019.
24. Shoujin Su, Philippe Zaza and Albert Renken, *Chemical Engineering & Technology*, 1994, **17**(1), 34.

25. N. Y. Usachev, I. M. Krukovskii and S. A. Kanaev, *Petroleum Chemistry*, 2004, **44**(6), 379.

26. M. Osugi and T. Uchiyama, *Process for the preparation for formaldehyde*, US Patent 4,054,609, 1977.

27. G. Wernet, C. Bauer, B. Steubing, J. Reinhard, E. Moreno-Ruiz and B. Weidema, *Int J Life Cycle Assess*, 2016, **21**(9), 1218.

28. GaBi, *GaBi 9.2.0.58: Software-System and Database for Life Cycle Engineering, DB 8.7 - SP 39*, thinkstep AG, Leinfelden-Echterdingen, Germany, 2019.

29. A. David, B. V. Mathiesen, H. Averfalk, S. Werner and H. Lund, *Energies*, 2017, **10**(4), 578.

30. L. J. Müller, A. Kätelhön, M. Bachmann, A. Zimmermann, A. Sternberg and A. Bardow, *Front. Energy Res.*, 2020, **8**, 1.

31. M. Reuß, T. Grube, M. Robinius, P. Preuster, P. Wasserscheid and D. Stolten, *Applied Energy*, 2017, **200**, 290.

32. S. Deutz and A. Bardow, *Nat Energy*, 2021.

33. N. von der Assen, L. J. Müller, A. Steingrube, P. Voll and A. Bardow, *Environmental science & technology*, 2016, **50**(3), 1093.

34. J. Burger, E. Ströfer and H. Hasse, *Chemical Engineering Research and Design*, 2013, **91**(12), 2648.

35. Eurostat, Passenger cars in the EU, https://ec.europa.eu/eurostat/statistics-explained/index.php/Passenger_cars_in_the_EU (last accessed January 2021).

36. S. Siegemund, M. Trommler, O. Kolb and V. Zinnecker, *E-fuels study: The potential of electricity-based fuels for low-emission transport in the EU: An expertise by LBST and dena*, Deutsche Energie-Agentur GmbH (dena), Berlin, 2017.